J|A|C|S ARTICLES

Published on Web 04/27/2009

Enrichment Mechanism of Semiconducting Single-Walled Carbon Nanotubes by Surfactant Amines

Sang-Yong Ju,[†] Marcel Utz,[†,‡,§] and Fotios Papadimitrakopoulos*[,†,⊥]

Nanomaterials Optoelectronics Laboratory (NOEL), Polymer Program, Institute of Materials Science, University of Connecticut, Storrs, Connecticut 06269

Received November 18, 2008; E-mail: papadim@mail.ims.uconn.edu

Abstract: Utilization of single-walled carbon nanotubes (SWNTs) in high-end applications hinges on separating metallic (*met*-) from semiconducting (*sem*-) SWNTs. Surfactant amines, like octadecylamine (ODA) have proven instrumental for the selective extraction of *sem*-SWNTs from tetrahydrofuran (THF) nanotube suspensions. The chemical shift differences along the tail of an asymmetric, diacetylenic surfactant amine were used to probe the molecular dynamics in the presence and absence of nanotubes via NMR. The results suggest that the surfactant amine head is firmly immobilized onto the nanotube surface together with acidic water, while the aliphatic tail progressively gains larger mobility as it gets farther from the SWNT. X-ray and high-resolution TEM studies indicate that the *sem*-enriched sample is populated mainly by small nanotube bundles containing ca. three SWNTs. Molecular simulations in conjunction with previously determined HNO_3/H_2SO_4 oxidation depths for *met*- and *sem*-SWNTs indicate that the strong pinning of the amine surfactants on the *sem*-enriched SWNTs bundles is a result of a well-ordered arrangement of nitrate/amine salts separated with a monomolecular layer of H_2O. Such continuous 2D arrangement of nitrate/amine salts shields the local environment adjacent to *sem*-enriched SWNTs bundles and maintains an acidic pH that preserves nanotube oxidation (i.e., $SWNT^{n+}$). This, in turn, results in strong interactions with charge-balancing NO_3^- counterions that through their association with neutralized surfactant amines provide effective THF dispersion and consequent *sem* enrichment.

Introduction

Single-walled carbon nanotubes (SWNTs) have drawn considerable attention from the scientific community based on their unique 1D electronic, optical and mechanical properties.[1] Their electronic structure depends strongly on the respective (*n,m*) indices, which exhibit metallic (*met*-) or semiconducting (*sem*-) behavior depending on whether or not the *n*-*m* reminder is an integer multiple of 3. A number of methodologies have come forward in order to separate *sem*- from *met*- SWNTs, among which the surfactant amine,[2] dielectrophoresis,[3] DNA-based ion-exchange chromatography,[4,5] and density-gradient centrifugation[6] routes present the most characterized embodiments.

In the case of amine-surfactant dispersion, the strong and localized ionic interactions between surfactant amines and carboxylic acids (located on the tips and side-walls of SWNTs) have been argued to assist nanotube dispersion in nonpolar aprotic media, such as THF (Scheme 1A).[7,8] It is now well-accepted that acid-induced treatment of SWNTs results in ~4−8 wt % of carboxylic functionalities.[9] However, a number of reports have raised strong indications that ionic complexes of carboxylic acid/surfactant amine base might not be the only contributor to the interactions of surfactant amines with SWNTs.[2,10,11] Our group proposed that the preferential interactions of octadecylamine (ODA) with *sem*-SWNTs is assisted by the cooperative effect between ionic (acid−base) and physisorbed surfactant anchoring, where the presence of the former stimulates the organization of the latter, as shown in Scheme 1B.[2] On a similar note, when oxidized SWNT are exposed to gaseous alkyl amines, the amount of amines incorporated is about an order of magnitude higher than that of the covalently bonded (amide) content in oxidized SWNTs.[10] More recently, the group led by Bao reported that self-assembled amine monolayers can preferentially attract *sem*-SWNTs and produce thin film transistors with large on/off ratios, consistent with semiconducting enriched samples.[11] Clearly, amine phy-

Scheme 1. Previously-Proposed Octadecylamine Interactions with SWNTS: (A) Zwitterions and (B) Physisorbed Amines along with Zwitterions

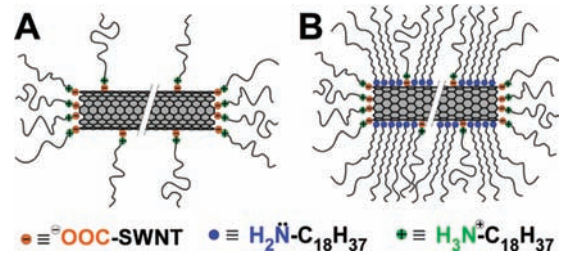

[†] Institute of Materials Science, University of Connecticut.
[‡] Department of Physics, University of Connecticut.
[§] Current address: Department of Mechanical and Aerospace Engineering, University of Virginia, Charlottesville, VA 22904-4746.
[⊥] Department of Chemistry, University of Connecticut.

(1) Dresselhaus, M. S.; Dresselhaus, G.; Avouris, P. *Carbon nanotubes: synthesis, structure, properties and applications*; Springer: Berlin, 2001.
(2) Chattopadhyay, D.; Galeska, I.; Papadimitrakopoulos, F. *J. Am. Chem. Soc.* **2003**, *125*, 3370–3375.
(3) Krupke, R.; Hennrich, F.; Lohneysen, H. v.; Kappes, M. M. *Science* **2003**, *301*, 344–347.

sisorption on the sidewall of SWNTs must be taken into account in order to explain the preferential enrichment of *sem*-SWNTs.

However, the physisorbed surfactant anchoring model lacks to account the driving force for overcoming the entropic barrier for surfactant amine organization. Clearly, the higher reactivity of *met*- over *sem*-SWNTs against oxidative treatment creates more carboxylic groups onto the sidewalls of *met*- as opposed to *sem*-SWNTs.[12] One potential explanation might be that higher concentration of carboxy functionalities onto *met*-SWNTs could disturb the organization of the surfactant-amine. Such model, however, can not address the specific diameter selective pattern of this enrichment.[13] More recently, a study from our group indicates that this enrichment appears to be intimately linked to the different level of oxidation that *sem*- and *met*-SWNTs experience when exposed to mixtures of HNO_3 and H_2SO_4 acid.[14] This explains the diameter dependence for this enrichment, as well as it links the electrochemical behavior of H_2O and O_2 at the vicinity of nanotubes to this enrichment process.

Nuclear magnetic resonance (NMR) has been instrumental in shedding more light to the local structure and dynamics of various molecules in confined architectures.[15,16] To this date, solution NMR behavior results involving carbon nanotube have shown that organic molecules attached on its sidewall experience: *i)* significant line broadening[17−19] *ii)* signal attenuation in close proximity to SWNTs,[18,19] and *iii)* upfield shifts for the nearby NMR-active nuclei attached to SWNTs.[17,20] In particular, using solid state ^{13}C NMR spectroscopy, Min Xu et al.,[21] reported the disappearance of the α, β and γ-methylene groups adjacent to the amine group of ODA, when reacted with the thionyl chloride-activated carboxylic functionalities of multiwall carbon nanotubes to form amide linkages.

In this contribution, nuclear magnetic resonance (NMR), differential scanning calorimetry (DSC), X-ray diffraction (XRD) and high-resolution transmission electron microscopy (HRTEM) characterization was employed to investigate in greater depth the local structure of nanotube/surfactant complex and its intramolecular dynamics in the presence and absence of H_2O. For this, the 5,7-eicosadiynoic amine (57ECA) surfactant was synthesized, in order to create chemical shift differences along the long fatty chain of the surfactant. ^1H and ^{13}C NMR studies suggested that the amine head is strongly immobilized onto the graphene sidewalls of SWNTs, along with the presence of acidic water. Upon closer inspection using XRD and HRTEM, the *sem*-enriched sample appears to be populated by small nanotube bundles containing three SWNTs. Molecular simulations in accordance with previously determined oxidation depths for *met*- and *sem*-SWNTs indicate that the strong immobilization of the amine surfactants on the side walls of these bundles is a result of a well-ordered arrangement of nitrate/amine salts separated with a monomolecular layer of H_2O. Such continuous 2D arrangement of nitrate/amine salts shields the local environment adjacent to *sem*-enriched SWNTs bundles and maintains an acidic pH. This, in turn, preserves nanotube oxidation (i.e., $SWNT^{n+}$) and results in strong interactions with charge-balancing NO_3^- counterions that through their association with neutralized surfactant amines provide effective THF dispersion. Such continuous 2D arrangement of hydrated nitrate/amine salts can be attained only from a specific type and diameter nanotubes in accordance with previously observed experimental results.[13,14] This explains the profound stability of the physisorbed amines (in their salt form) on the nanotube bundle, which provides a noncovalent, "hairy-rod" nature to a very rigid structure and renders it dispersible in THF. These finding provides the missing link on the interaction of surfactant amines with *sem*-SWNTs and shed more light on the localized electrochemistry of nanostructured materials.

Experimental Section

Materials and Instrumentation. Single-walled carbon nanotubes prepared by the HiPco process[22] were purchased from Carbon Nanotechnology Inc. (lot # CN1003). 5,7-Eicosadiynoic acid (**1**) was purchased from GFS chemicals. 99.8 atom % deuterated D_2O was purchased from Acros. Both deuterated tetrahydrofuran (99.5 atom % deuterated, THF-d_8) and tetramethylsilane (TMS, 99.9%) were obtained from Sigma Aldrich. All remaining solvents and chemicals were reagent grade and used as received. All Raman spectra were collected with a Renishaw Raman scope in the backscattering configuration. SWNTs resonance Raman spectroscopy was conducted in Stokes mode using 514.5 nm (2.41 eV) excitation lasers source. Prior to the collection of Raman spectra, all drop-cast samples were vacuum-dried (less than 1 Torr) at 300 °C to sublime all residual 57ECA molecules that contribute substantial background luminescence,[23] and further eliminates any possible interferences from the surfactant to the electronic structure

(4) Zheng, M.; Jagota, A.; Semke, E. D.; Diner, B. A.; McLean, R. S.; Lustig, S. R.; Richardson, R. E.; Tassi, N. G. *Nat. Mater.* **2003**, *2*, 338–342.
(5) Zheng, M.; Jagota, A.; Strano, M., S.; Santos, A., P.; Barone, P.; Chou, S. G.; Diner, B., A.; Dresselhaus, M., S.; McLean, R., S.; Onoa, G. B.; Samsonidze, G. G.; Semke, E., D.; Usrey, M.; Walls, D., J. *Science* **2003**, *302*, 1545–1548.
(6) Arnold, M. S.; Green, A. A.; Hulvat, J. F.; Stupp, S. I.; Hersam, M. C. *Nat. Nanotechnol.* **2006**, *1*, 60–65.
(7) Hamon, M. A.; Chen, J.; Hu, H.; Chen, Y.; Itkis, M. E.; Rao, A. M.; Eklund, P. C.; Haddon, R. C. *Adv. Mater.* **1999**, *11*, 834–840.
(8) Liu, J.; Rinzler, A. G.; Dai, H.; Hafner, J. H.; Bradley, R. K.; Boul, P. J.; Lu, A.; Iverson, T.; Shelimov, K.; Huffman, C. B.; Rodriguez-Macias, F.; Shon, Y.-S.; Lee, T. R.; Colbert, D. T.; Smalley, R. E. *Science* **1998**, *280*, 1253–1256.
(9) Hamon, M. A.; Hu, H.; Bhowmik, P.; Niyogi, S.; Zhao, B.; Itkis, M. E.; Haddon, R. C. *Chem. Phys. Lett.* **2001**, *347*, 8–12.
(10) Basiuk, E. V.; Basiuk, V. A.; Banuelos, J.-G.; Saniger-Blesa, J.-M.; Pokrovskiy, V. A.; Gromovoy, T. Y.; Mischanchuk, A. V.; Mischanchuk, B. G. *J. Phys. Chem. B* **2002**, *106*, 1588–1597.
(11) LeMieux, M. C.; Roberts, M.; Barman, S.; Jin, Y. W.; Kim, J. M.; Bao, Z. *Science* **2008**, *321*, 101–104.
(12) Zhang, G.; Qi, P.; Wang, X.; Lu, Y.; Li, X.; Tu, R.; Bangsaruntip, S.; Mann, D.; Zhang, L.; Dai, H. *Science* **2006**, *314*, 974–977.
(13) Samsonidze, G. G.; Chou, S. G.; Santos, A. P.; Brar, V. W.; Dresselhaus, G.; Dresselhaus, M. S.; Selbst, A.; Swan, A. K.; Unlu, M. S.; Goldberg, B. B.; Chattopadhyay, D.; Kim, S. N.; Papadimitrakopoulos, F. *Appl. Phys. Lett.* **2004**, *85*, 1006–1008.
(14) Kim, S. N.; Luo, Z.; Papadimitrakopoulos, F. *Nano Lett.* **2005**, *5*, 2500–2504.
(15) Panich, A. M. *Diamond Relat. Mater.* **2007**, *16*, 2044–2049.
(16) Mallamace, F.; Corsaro, C.; Broccio, M.; Branca, C.; Gonzalez-Segredo, N.; Spooren, J.; Chen, S. H.; Stanley, H. E. *Proc. Natl. Acad. Sci. U.S.A.* **2008**, *105*, 12725–12729.
(17) Holzinger, M.; Vostrowsky, O.; Hirsch, A.; Hennrich, F.; Kappes, M.; Weiss, R.; Jellen, F. *Angew. Chem., Int. Ed.* **2001**, *40*, 4002–4005.
(18) Holzinger, M.; Abraham, J.; Whelan, P.; Graupner, R.; Ley, L.; Hennrich, F.; Kappes, M.; Hirsch, A. *J. Am. Chem. Soc.* **2003**, *125*, 8566–8580.
(19) Star, A.; Stoddart, J. F.; Steuerman, D.; Diehl, M.; Boukai, A.; Wong, E. W.; Yang, X.; Chung, S.-W.; Choi, H.; Heath, J. R. *Angew. Chem., Int. Ed.* **2001**, *40*, 1721–1725.
(20) Chen, J.; Liu, H.; Weimer, W. A.; Halls, M. D.; Waldeck, D. H.; Walker, G. C. *J. Am. Chem. Soc.* **2002**, *124*, 9034–9035.
(21) Xu, M.; Huang, Q.; Chen, Q.; Guo, P.; Sun, Z. *Chem. Phys. Lett.* **2003**, *375*, 598–604.
(22) Nikolaev, P.; Bronikowski, M. J.; Bradley, R. K.; Rohmund, F.; Colbert, D. T.; Smith, K. A.; Smalley, R. E. *Chem. Phys. Lett.* **1999**, *313*, 91–97.
(23) Lin, Y.; Taylor, S.; Huang, W.; Sun, Y. P. *J. Phys. Chem. B* **2003**, *107*, 914–919.

of SWNTs. Nanotube diameter and wavenumber were correlated using $\omega_{RBM} = \alpha/d_t + \beta$, where α and β are 223.5 cm^{-1} nm and 12.5 cm^{-1}, respectively.[24] Differential scanning calorimetry (DSC) was performed on a DSC 2920 (TA Instruments) at a ramping rate of 5 °C/ min, using a liquid DSC pan. X-ray diffraction was collected using Bruker D8 Avance using Cu Kα source (1.54 Å). Gas chromatography−mass spectrometry (GC−MS) was conducted using a Hewlett-Packard 5890 and 6890 series equipped with a custom-made injection head to confirm the purity of various chemicals. Transmission electron microscopy (TEM) characterization was performed using a JEOL JEM-2010 electron microscope, operating at 200 kV.

Synthesis: 5,7-Eisosadiynoic Acid Chloride (2) and 5,7-Eisosadiynoic Amide (3). A catalytic amount of *N*,*N*-dimethylformamide (DMF) was added dropwise into a mixture of 2.5 g (20 mmol) of oxalyl chloride, 2.0 g (3.3 mmol) of 5,7-eicosadiynoic acid (**1**) in 20 mL of anhydrous methylene chloride (MC). The solution was stirred at room temperature for 2 h. The organic solvent was then rotary-evaporated to give a white viscous fluid containing compound **2**. This was used in the next step without further purification (yield: 2.12 g, 99%).

2, 2.12 g in 10 mL of anhydrous THF, was added for 15 min dropwise to 100 mL of the ammonium hydroxide solution (28 wt % aqueous solution) at 0 °C under vigorous stirring. The resulting white solid was filtered and washed several times with distilled water. The resulting solid was put into a thimble together with magnesium sulfate and was extracted from 400 mL of diethyl ether using a Soxhlet apparatus. After extracting for 1 day, the extract was placed into a refrigerator and allowed to precipitate white flaky crystals of compound **3**. The filtered solid produce ~1.88 g (yield: 95%) of compound **3**: mp 116−118 °C, (From DSC, 120 °C), ^{1}H NMR ($CDCl_3$ with TMS as a internal reference) δ 0.88 (t, J = 7.0 Hz, 3H, -CH_3), 1.26 (br m, 6H, -CH_2-), 1.37 (br m, 2 H, -CH_2-), 1.52 (q, J = 7.65 Hz, 2 H, -CH_2-), 1.88 (q, J = 7.0 Hz, 2 H, -CH_2-), 2.25 (t, J = 7 Hz, 2H, triplet), 2.37 (t, J = 6.63 Hz, 2H, -CH_2−C≡), 2.41 (t, J = 7.4 Hz, 2 H, -CH_2−C≡), 5.90 (br s, 2H, -NH2); ^{13}C NMR ($CDCl_3$ with TMS as a internal reference) δ 14.12, 18.62, 19.22, 22.72, 23.79, 28.33, 28,89, 29.13, 29.37, 29.51, 29.65, 31.94, 34.13, 65.04, 66.36, 76.03, 76.52, 174.35; IR (neat film on KBr pellet) ν (cm^{-1}) 3371, 2955, 2918, 2848, 1649, 1458, 1426, 722, 685; GC−MS Calcd. for $C_{20}H_{33}NO$ *m*/*z* 303.26, 304.26, 305.26, Obtained 303.3, 304.2, 305.2; Elemental Analysis: Anal. Calcd. for $C_{20}H_{33}NO$ (FW: 303.48): C, 79.15; H, 10.96; N, 4.62; O, 5.27. Found: C, 79.36; H, 11.31; N, 4.59, O, 5.53.

5,7-Eicosadiynoylamine (57ECA). A quantity of 0.748 g (26 mmol) of lithium aluminum hydride was slowly added to a solution of 1.5 g (4.9 mmol) of **3** in 100 mL of diethyl ether, and the reaction was refluxed overnight. The reaction was terminated by quenching the excess hydride with careful addition of distill water until no further gas evolution was observed, while the flask was kept cold into an ice bath. The organic solvents were rotary-evaporated to produce a viscous yellow liquid. A thin layer chromatography (TLC) with a 1:1 mixture of MC:methanol yields an R_f value of the target compound of approximately 0.11, which could be visualized by the brown color using ninhydrin test.[25] Purified 57ECA was obtained from subsequent silica gel column chromatography with the similar elusion composition as the case of TLC developer. Following rotary evaporation of the organic solvents, 1.0 g of a yellowish-white liquid was obtained with a yield of 70%. In order to obtain water-free 57ECA, the aforementioned liquid was microdistilled at reduced pressure (0.1 mmHg) to produce neat (water-free) 57ECA that crystallized at low temperature. (mp: 18 °C). ^{1}H NMR (THF-d_8 with TMS as a internal reference) δ 0.89 (t, J = 6.89 Hz, 3H, -CH_3), 1.26 (br m, 18H, -CH_2-), 1.37 (br m, J = 6.9 Hz, 2H, -CH_2-), 1.47 (q, 2H, -CH_2-), 1.49 (q, J = 6.9 Hz, 2H, -CH_2-), 1.51 (q, J = 5.5 Hz, 2H, -CH_2-), 2.225 (t, J = 6.6 Hz, 2H, -CH_2-C≡), 2.238 (t, J = 6.4 Hz, 2H, -CH_2-C≡), 2.61(t, J = 7.4 Hz, 2H, -CH_2-NH_2); ^{13}C NMR (THF-d_8 with TMS as a internal reference) δ 14.44, 19.52, 19.58, 23.57, 26.80, 29.43, 29.77, 30.09, 30.32, 30.49, 30.59, 30.62, 32.88, 33.99, 42.56, 66.41, 75.76, 77.43, 77.56; IR (neat film on KBr pellet) ν (cm^{-1}) 3378, 3259, 2925, 2854, 1663, 1623, 1576, 1464, 1335, 1080, 722; GC−MS Calcd. for $C_{20}H_{35}N$ *m*/*z* 289.28, 290.28, Obtained 289.3, 290.3.; Elemental Analysis: Anal. Calcd. for $C_{20}H_{35}N$ (FW: 289.50): C, 82.98; H, 12.19; N, 4.84. Found: C, 82.98; H, 12.36; N, 4.70.

Preparation of Solid 57ECA Sample. 57ECA solution in *n*-hexane was subject to flow onto a humidified slide glass. Multiple times of this process leave a white solid film onto the slide glass, which was collected by razor blade and vacuum-dried at room temperature to produce solid 57ECA.

Acid Treatment of SWNTs (a-SWNTs). HiPco SWNTs were treated by sonication-assisted oxidation in a mixture of H_2SO_4 (96%) and HNO_3 (98%) according to the established methods.[2,8,26] 100 mg of SWNT were introduced into 40 mL of a 3:1 vol. mixture of H_2SO_4 and HNO_3. The resulting black solution was mildly sonicated for 4 h to allow SWNT to be shortened and functionalized with carboxylic groups. Following this, the nanotube suspension was filtered with 0.45 μm Teflon filter and washed with copious amount of distilled water until the pH of the filtrate has reached a value of 6. The resulting SWNT mat was peeled and vacuum-dried at 60 °C for 1 day to give acid-treated SWNTs.

Functionalization of a-SWNT with 57ECA (57ECA−SWNT) and Dispersion of 57ECA−SWNT in THF. The functionalization process involves mixing 5 mg of acid-treated SWNTs with 100 mg of 57ECA into an amber-colored vial under argon and maintained for 5 days while heating at 95 °C. The mixture was allowed to cool down at room temperature and was briefly sonicated in ethanol and the solid was collected by filtration and dried in vacuum (wash step to remove free 57ECA). The dried black solid was then placed in 20 mL of THF and bath-sonicated (80 W intensity) for 1 h, and the dispersion was allowed to stand at room temperature for one day, in order to settle any precipitates. The supernatant was carefully collected and used in this study, while a substantial amount (i.e., 80−85%) of the aforementioned solid remained nonsuspended. ODA was similarly functionalized with a-SWNTs, according to the aforementioned methods.

Preparation of HCl-Acidified D_2O. Partially deuterated HCl-acidified D_2O was prepared according to the literature.[27] Aqueous HCl solution (38%) was dropwise added into first H_2SO_4 (98%), in which the generated HCl gas was again introduced into second H_2SO_4 (98%) vessel, to remove any remaining water. The passed HCl gas was trapped into D_2O solution for 30 min. This HCl-acidified D_2O solution was diluted with D_2O to prepare different pH solutions (i.e., pH 2, 3, 4, and 5).

NMR Spectroscopy. NMR spectra were acquired on a Bruker DMX spectrometer operating at a proton Larmor frequency of 400 MHz. THF-d_8 was dried over molecular sieve (4 Å) for one day, prior to NMR measurement. All spectra were recorded with 5 mm NMR tube containing 4.9 mM of tetramethylsilane (TMS) in 0.6 mL of THF-d_8 at 25 °C, unless otherwise mentioned. In the case of the NMR sample, around 1.55 mg of 57ECA−SWNTs was introduced into a vial containing 1 mL of THF-d_8, and the heterogeneous solution was dispersed using the bath-sonicator and was allowed to settle any precipitates while this solution was being dried over 4 Å molecular sieves. The supernatant was carefully collected and was introduced into a NMR tube. In order to prevent H_2O absorption, two sealed NMR tubes including neat 57ECA at 8.6 and 69 mM in THF-d_8 were prepared for ^{1}H−^{1}H correlation

(24) Bachilo, S. M.; Strano, M. S.; Kittrell, C.; Hauge, R. H.; Smalley, R. E.; Weisman, R. B. *Science* **2002**, *298*, 2361–2366.
(25) Nelson, D. L.; Cox, M. M. *Lehninger Principles of Biochemistry*, 3rd ed.; Worth Publishers Inc.: New York, 2003.
(26) Ju, S. Y.; Papadimitrakopoulos, F. *J. Am. Chem. Soc.* **2008**, *130*, 655–664.
(27) Vogel, A. I.; Tatchell, A. R.; Furnis, B. S.; Hannaford, A. J.; Smith, P. W. G. *Vogel's Textbook of Practical Organic Chemistry*, 5th ed.; Prentice Hall: New York, 1996; p 438.

Scheme 2. Synthetic Route of 57ECA[a]

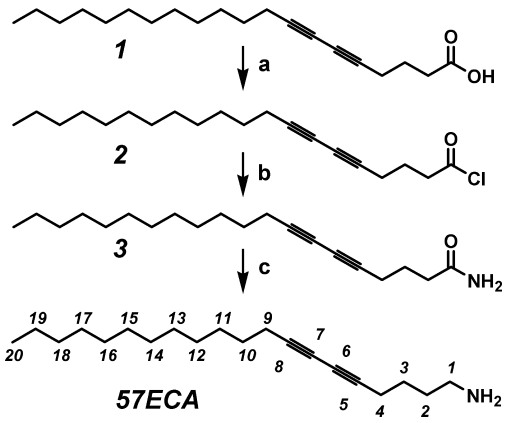

[a] Conditions: (a) $(COCl)_2$/DMF/CH_2Cl_2, rt, 2 h; (b) NH_4OH/water, 0 °C; (c) $LiAlH_4$/diethyl ether, reflux, overnight.

spectroscopy (2D COSY) and $^1H-^{13}C$ heteronuclear multiple bond correlation (HMBC) experiments, respectively. For temperature-controlled measurements, all samples were kept at each temperature for at least 20 min prior to spectra collection to allow thermal and convectional equilibration. Chemical shift (δ) and line-width monitoring experiment in the presence of D_2O were conducted using NMR tube with a rubber septum, where D_2O was carefully introduced in a 0.5 μL portions. Spin−lattice relaxation measurements were obtained by inversion recovery. The resulting relaxation curves were constructed from the randomized 12 time entries (i.e., 60, 2, 0.1, 0.5, 5, 30, 0.3, 15, 8, 0.8, 1, 1.5 s).

Molecular Modeling. Cerius2 simulation software was utilized for molecular modeling using the Dreiding 2.21 force field for molecular mechanics, molecular dynamics and quenched dynamics simulations, as detailed elsewhere.[28] Materials Studio 4 software was used for visualization. A hydrated NO_3^- geometry with sp^3 configuration was reconstructed according to the literature.[29]

Results

Octadecylamine (ODA) has been instrumental for attaining *sem*- to *met*-SWNT enrichement.[2,13] The similar chemical shifts for ^1H and ^{13}C NMR atoms located in the middle section of ODA, however, limits us from exploring its intramolecular dynamics within its neat- as well as nanotube-functionalized states. After a number of trial and errors we have arrived to the 5,7-eicosadiynoylamine (57ECA) (see Scheme 2), imparting the adequate chemical anisotropy due to the asymmetric insertion of the diacetylenic moiety in fifth carbon of a 20 carbon-long chain. The additional two carbon atoms, compared to the 18 carbon of the ODA, were needed to raise its melting point comparable to ODA. This compound was synthesized *via* a facile three step reaction, in accordance to a previously reported protocol.[30] The starting 5,7-eicosadiynoic acid (**1**) was reacted with oxalyl chloride to yield 5,7-eicosadiynoic acid chloride (**2**). This acid chloride (**2**) was further reacted with ammonium hydroxide, to generate compound **3** in an almost quantitative yield. This amide compound **3** was carefully reduced to 57ECA by using $LiAlH_4$. Here it is important to mention that all diacetylenic compounds were handled and stored under a yellow light to prevent possible polymerization.[31]

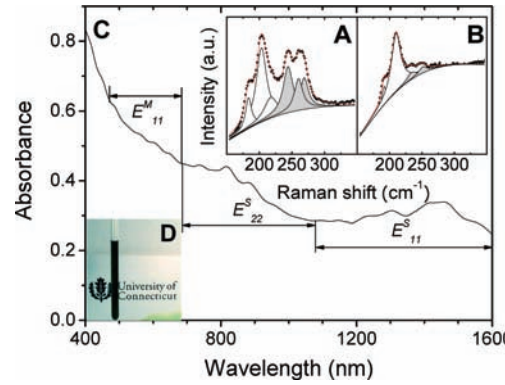

Figure 1. (A and B) Resonance Raman spectra of the radial breathing mode (RBM) region of acid-treated SWNTs before (A) and after (B) 57ECA-assisted enrichment. Prior to spectral collection using 514 nm laser excitation, both samples were vacuum-annealed at 300 °C to remove all absorbates including 57ECA. Black circles and red lines denote the experimental and summated data following peak deconvolution using Lorentzian line shapes. White and gray peaks indicate *sem*- and *met*-SWNT constituents, respectively. (C) UV−vis−NIR spectrum of 57ECA-enriched nanotubes dispersed in THF. (D) Optical image of an NMR tube containing a stable, 57ECA-dispersed nanotube suspension in THF-d_8.

HiPco SWNTs were oxidized with a 1:3 v/v mixture of HNO_3 and H_2SO_4 *via* 4 h sonication. This step has been shown to: (i) shorten,[32] (ii) oxidize (p-dope) SWNTs,[8] and (iii) add COOH functionality[10] onto SWNTs. The nanotube solution was filtered, and the filtrated nanotubes were washed several times with water until the filtrate reaches a pH ~6. Spectroscopic evidence indicate that these nanotubes retain their *p*-doped state, which is locked within small bundles.[14] The oxidized nanotube was vacuum-dried at 60 °C to remove the majority of water, yet some H_2O is inevitably retained. Subsequently, the nanotubes were mixed with 57ECA and annealed under argon at 95 °C for 5 days. This prompted nanotube exfoliation that produces a heavily dark, homogeneous suspension. Since 57ECA, like ODA, is partially soluble in ethanol, excess of 57ECA was removed by a brief sonication step in ethanol, followed by nanotube filtration and vacuum-drying at 60 °C. Subsequently, the 57ECA-treated nanotube sample was dispersed in THF via 1 h sonication, and the solution was kept for 1 day before carefully decanting the supernatant that contains *sem*-enriched SWNTs.

Spectroscopic Characterization. Parts A and B of Figure 1 illustrate the radial breathing mode (RBM) of 514 nm excited SWNTs before (A) and after (B) 57ECA treatment. This excitation enables us to probe the E^S_{44} of large diameter (d_t) semiconducting (d_t ranging from 1.15 to 1.3 nm) and E^M_{11} of small d_t metallic (d_t ranging from 0.9 to 1.15 nm) transitions of HiPco SWNTs.[24] Here it is important to mention that (i) the spectrum of Figure 1A originates from the acid-treated nanotube sample, and (ii) both samples were vacuum-annealed at 300 °C to remove any remaining absorbates, like acids, H_2O and 57ECA. While the acid-treated sample contains both metallic and semiconducting species, 57ECA-treated sample shows enrichment mainly from the semiconducting portion. These results are in accordance with ODA-induced separation, indicating that 57ECA behaves similar to ODA.[2]

Figure 1C illustrates the UV−vis−NIR absorption spectrum of THF-suspended 57ECA−SWNTs. In accordance with the

(28) Ju, S.-Y.; Doll, J.; Sharma, I.; Papadimitrakopoulos, F. *Nat. Nanotechnol.* **2008**, *3*, 356–362.
(29) Kameda, Y.; Saitoh, H.; Uemura, O. *Bull. Chem. Soc. Jpn.* **1993**, *66*, 1919–1923.
(30) Walsh, S. P.; Lando, J. B. *Langmuir* **1994**, *10*, 252–256.
(31) Ahn, D. J.; Kim, J.-M. *Acc. Chem. Res.* **2008**, *41*, 805–816.
(32) Gooding, J. J.; Wibowo, R.; Liu, J.; Yang, W.; Losic, D.; Orbons, S.; Mearns, F. J.; Shapter, J. G.; Hibbert, D. B. *J. Am. Chem. Soc.* **2003**, *125*, 9006–9007.

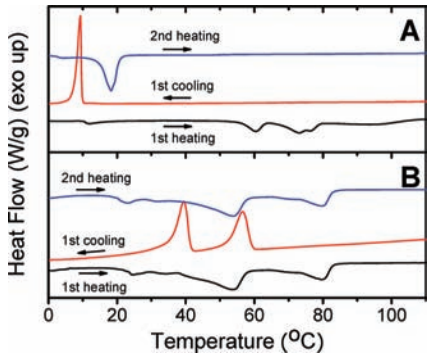

Figure 2. Five °C/min differential scanning calorimetry (DSC) thermohistograms of 57ECA in the absence (A) and presence (B) of SWNTs. The first heating scan of Figure 2A originates from a H_2O-containing 57ECA sample (see text for details).

aforementioned resonance Raman results, both E^S_{22} (680 to 1100 nm) and E^S_{11} (1000 to 1600 nm) transitions are substantially bigger than the E^M_{11} (470 to 680 nm) transitions of *met*-SWNTs. The small peaks at 566, 606, 651 nm indicate that large d_t *met*-SWNTs are also present in agreement with previously reported results.[2,13] The E^S_{11} absorptions are significantly less resolved than SDS-dispersed nanotube sample,[33] providing a qualitative assessment of its lightly bundled state.[4,20,33] Figure 1D depicts an optical image of an NMR tube with the 57ECA−SWNTs suspension in THF-d_8 under investigation. The black appearance of this suspension is indicative of the significant amount of nanotubes suspended with 57ECA. A high-resolution TEM (HRTEM) image in Figure S1 in the Supporting Information (SI) provides additional verification of their lightly bundled state.

Thermal and Structural Characterization. Typically 57ECA is a viscous liquid at room temperature. A prior report indicated that when alkyl amines are brought in contact with water, higher-temperature liquid crystalline phases are formed.[34] Following this finding, we solvent-cast *n*-hexane solutions of 57ECA onto a moistened glass surface to obtain a white crystalline solid. This solid was scraped off, vacuum-dried at room temperature, and subjected to DSC investigation as shown in Figure 2A. Multiple attempts using flame-dried sublimation setup failed to obtain the solid 57ECA sample, which suggests that water plays a important role in formation of solid sample. The first heating scan indicates the presence of a small endotherm (∼12 °C) followed by multiple, higher-temperature endotherms, between 50 and 80 °C. When this sample is subjected to cooling, only a low-temperature exotherm was observed. Subsequent heating indicated a T_g around 5 °C, followed by a profound low-temperature endotherm peaking at 18 °C. Neat 57ECAs (devoid of water) have shown similar DSC thermohistograms with the second heating scan (data not shown), confirming its viscous liquid nature at room temperature. The water association with high-temperature endotherms is also confirmed from Figure 2A since, upon evaporating the H_2O (at temperatures greater than 100 °C) at the end of the first heating scan, high-temperature transitions were absent in the subsequent heating scan.

Wide angle X-ray diffractometry (WAXD) was utilized to shed more light to the high-temperature order phase of

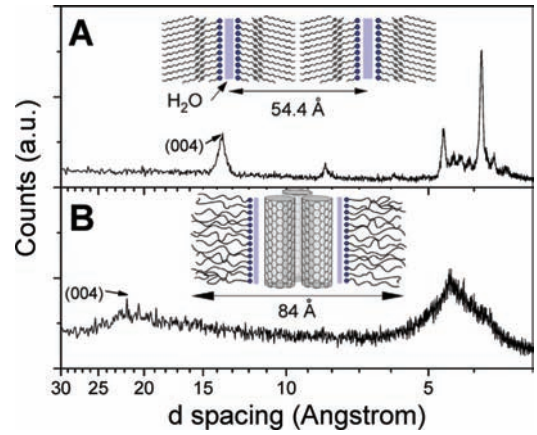

Figure 3. Wide-angle X-ray diffraction of the high-melting point 57ECA−H_2O structure (A) and 57ECA−SWNT (B). Insets portray the schematic organization of these complexes, with the blue solid lines indicating the location of water (close pack arrangement of the 57ECA amine heads on the sidewalls of SWNTs is supported by subsequent NMR and molecular simulations results).

57ECA−H_2O. The elimination of the low-temperature crystalline phase (T_m = 18 °C) was easily accomplished by performing WAXD at room temperature (∼25 °C). The strong 13.6 Å peak was indexed to the (004) longitudinal diffraction, based on the presence of four symmetry points, two of them originating from the diacetylene kinks and the other two from the 57ECA termini.[35] Since 57ECA molecule is 28.5 Å long, the 54.4 Å (001) spacing suggests a slightly tilted herringbone type of structure (inset in Figure 3A), with significant lateral order as suggested by the multiplicity of diffraction peaks between 3 and 5 Å. The lack of higher-order longitudinal diffractions (i.e., (006) and (008) at 9.1 and 6.8 Å, respectively) suggests that the high-temperature 57ECA−H_2O phase belongs to higher-order smectic phase, in accordance with a previous report.[34]

Figure 2B illustrates heating and cooling DSC scans of 57ECA in the presence of SWNTs. In the first heating scan, a multiplicity of endotherms is observed, with the more pronounced endotherms peaking at 24, 54, and 81 °C. When this sample was cooled, supercooled exotherms corresponding to the 54 and 81 °C melting peaks were observed. On the second heating scan, all endothermic transitions of the first heating scan were observed without any diminution in their ΔH values. Unlike the 57ECA−H_2O case of Figure 2A, the 57ECA−SWNT complexes exhibit profound stability of their underlying order, amid a strong tendency to also retain any residual H_2O. Figure 3B depicts the corresponding WAXD results of 57ECA in the presence of SWNTs. The much broadened diffraction peaks indicate a higher degree of disorder. Utilizing the same formalism with the higher-temperature 57ECA−H_2O smectic phase, the peak at 21 Å was similarly assigned to the (004) order. Unlike the lamellar 57ECA arrangement, the one-dimensional (1D) character of SWNTs is expected to adopt a hexagonal lateral arrangement, with the 57ECA chains bending to accommodate close-packing. With a (001) spacing in the order of 84 Å, and assuming a 57ECA length slightly less than 54.4 Å (due to the trigonal disorder), a remaining 30−35 Å suggests the presence of a small SWNT bundle that consists of about 3 close-packed nanotubes. This is consistent with the

(33) O'Connell, M. J.; Bachilo, S. M.; Huffman, C. B.; Moore, V. C.; Strano, M. S.; Haroz, E. H.; Rialon, K. L.; Boul, P. J.; Noon, W. H.; Kittrell, C.; Ma, J.; Hauge, R. H.; Weisman, R. B.; Smalley, R. E. *Science* **2002**, *297*, 593–596.
(34) Ralston, A. W.; Hoerr, C. W.; Hoffman, E. J. *J. Am. Chem. Soc.* **1942**, *64*, 1516–1523.
(35) Yang, Y.; Lu, Y.; Lu, M.; Huang, J.; Haddad, R.; Xomeritakis, G.; Liu, N.; Malanoski, A. P.; Sturmayr, D.; Fan, H.; Sasaki, D. Y.; Assink, R. A.; Shelnutt, J. A.; van Swol, F.; Lopez, G. P.; Burns, A. R.; Brinker, C. J. *J. Am. Chem. Soc.* **2003**, *125*, 1269–1277.

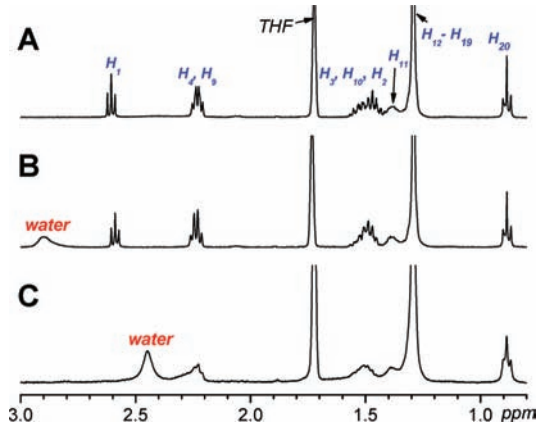

Figure 4. ^{1}H NMR spectra of 57ECA in the (A) absence and (B) presence of water. (**C**)^{1}H NMR spectrum of 57ECA-treated SWNTs, which are suspended in THF-d_8.

HRTEM results of Figure S1 (in SI) along with the UV−vis-NIR data of Figure 1C.

NMR Characterization. The peak assignments of various proton and carbon species within the aliphatic tail of 57ECA were accomplished on the basis of the known chemical shifts and inductive effects of functional groups.[36] This has been confirmed using ^{1}H−^{1}H 2D-correlation spectroscopy (COSY) and ^{1}H−^{13}C heteronuclear multiple bond correlation (HMBC) as shown in Figures S2 and S3 in the SI, respectively. Figure S4 in the SI provides a close-up of the C_{10} to C_{17} region that is not easily visualized in Figure S3, SI. Based on this analysis, all carbon species and the majority of proton species of 57ECA have been visualized and successfully assigned, according to the numbering shown in Scheme 2. In particular, H_1 and H_{20} are isolated, while H_4/H_9, $H_3/H_2/H_{10}$, H_{11}-H_{19} are bundled within three separate peaks.

Parts A and B of Figure 4 show the ^{1}H NMR of 57ECA in the absence (A) and presence (B) of water, dissolved in anhydrous THF-d_8. Particular care was exerted to remove water from 57ECA using vacuum distillation and storing it within desiccated vials. When water is not present, 57ECA exhibits a ^{1}H NMR spectrum with a narrow line-width (i.e., 1.5 and 1.4 Hz for H_1 and H_{20} peak, respectively). In the presence of water, ^{1}H NMR of 57ECA shows a slight peak broadening (i.e., 1.7 and 1.5 Hz for H_1 and H_{20} peaks, respectively). This broadening appears to be greater for the protons closer to the amine functionality. In addition, the H_1 peak is rather upfield-shifted (by *ca.* 0.02 ppm) with respect to the neat 57ECA. This provides an initial indication that H_2O (whose chemical shift is shown within a broad peak at 2.9 ppm) is preferentially associated with the amine group of 57ECA and results in partial restriction of the mobility of its nearly H_1.

Figure 4C illustrates the ^{1}H NMR of 57ECA-treated SWNTs. This sample has a deep black appearance (Figure 1D), which indicates that considerable amounts of SWNTs are dispersed within the anhydrous THF-d_8 solvent. As expected, the resulting ^{1}H NMR spectrum is substantially broadened, and the H_1 peak has completely disappeared. In the presence of SWNTs, the line width (3.8 Hz) of the terminal H_{20} proton is 2.5 times higher than that of neat 57ECA (i.e., 1.4 Hz). In the case of the composite H_4/H_9 peak, the H_4 contribution appears substantially broadened, while the H_9 peak exhibits a line width of 6.5 Hz as opposed to 3.7 Hz for neat 57ECA. Most interesting, however, is the position of the broad H_2O peak that in the presence of SWNTs shows a dramatic (0.5 ppm) upfield shift to 2.4 ppm.

In order to elucidate the nature of the water peak shift, we added 20 μL of HCl-acidified D_2O with varying pH values (i.e., 2, 3, 4 and 5) to the neat 57ECA THF-d_8 solution. Figure S5 of the SI depicts the ^{1}H NMR spectra of 57ECA as a function of the pH values of the added HCl-acidified D_2O. The water peak is gradually upshifted and sharpened at lower pH values and in the case of pH of 2 addition of HCl-acidified D_2O it peaked at a value of 2.8 ppm.[37] As expected, the overwhelming amount of 57ECA within the THF-d_8 solution neutralizes the majority of HCl. In the case of SWNT, the observed 2.4 ppm value indicates that this water is considerably acidic. In order to determine whether this water is evenly distributed within the suspension or locally resides at the vicinity of SWNTs, we have added 4 Å molecular sieves to the 57ECA/SWNT in THF-d_8 suspension. Failure to remove or even lower the signal originating from water indicates that this acidic water is located at the vicinity of carbon nanotubes. This suggests that acid/base interactions between acidic water and basic 57ECA surfactant amine might be the reason for the strong association of the amine headgroup onto the nanotubes, with such ionic bond stabilized due to the low dielectric constant of the surrounding THF environment.

Since the H_1 shift of 57ECA is situated close to the broad and pH-dependent resonance of H_2O in Figure 4, it is important to ensure that in the case of 57ECA−SWNT (Figure 4C), the particular proton is absent and not buried underneath the water peak. For this we utilized ODA as opposed to 57ECA, since the H_1 triplet is far away from other proton peaks, such as the H_4 and H_9 of 57ECA. Figure S6(A) of the SI illustrates the ^{1}H NMR spectrum of neat ODA in anhydrous THF-d_8, with the H_1 triplet centered at 2.58 ppm, which is the exactly same position with that of 57ECA. B and C of Figure S6 of the SI depict the ^{1}H NMR spectra of ODA-treated SWNT at 27 and 57 °C, respectively. Acquiring the ODA-SWNT spectrum at different temperatures, enabled us to shift the H_2O peak away from the chemical shift of H_1, while all other protons remain unchanged.[16] The absence of the H_1 triplet in both temperatures suggests that the amine surfactants are strongly anchored on the nanotube side-walls and this complex is stable at 57 °C (close to the boiling point of THF).

As shown in both DSC and XRD studies, the amount of H_2O plays a strong role to the ordering of surfactant amines in the condensed state. In order to elucidate the effect of H_2O in the dissolved state, we investigated the peak position and line broadening of the terminal protons of 57ECA (*i.e.,* H_1 and H_{20}) protons as a function of water concentration. Figure 5 depicts the peak positions (open circles and squares for H_1 and H_{20}, respectively) along with line broadening (shown by error bars) as a function of D_2O concentration, given in both D_2O/THF volume and D_2O/57ECA molar ratio (shown in bottom and top abscissa, respectively). While the chemical shift and line width of H_{20} remain almost constant upon addition of D_2O, the same is not observed for the H_1 peak. The H_1 proton first experiences a rapid upfield (until ~0.0027 D_2O/THF volume ratio corresponding to ~2−3 molecules of water per amine, shown with an arrow #1), which is then followed by a more gradual upfield shift before reaching a plateau (shown with an arrow #2). Similarly, the increase in line broadening follows these two

(36) Pavia, D. L.; Lampman, G. M.; Kriz, G. S. *Introduction to Spectroscopy*, 3rd ed.; Brooks Cole: 2000.

(37) Farcasiu, D.; Ghenciu, A. *J. Am. Chem. Soc.* **1993**, *115*, 10901–8.

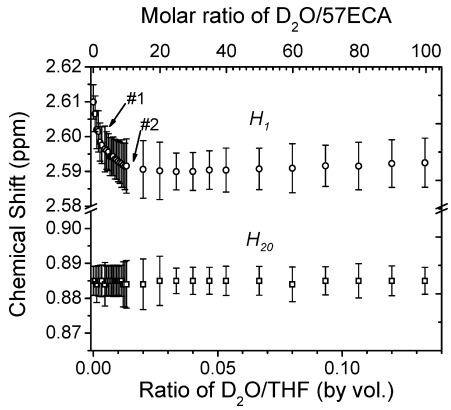

Figure 5. Chemical shift and line width variation of H_1 and H_{20} peaks, as a function of increasing D_2O concentration in THF-d_8. Open circles and squares denote the chemical shifts of peaks, respectively. Error bars depict the corresponding line-broadening values of the H_1 and H_{20} peaks.

regimes and records a 10 and 56% raise (at the aforementioned arrow points), when compared with the neat value of 57ECA. This behavior is indicative of the water-assisted colloidal surfactant organization of 57ECA in 8.6 mM THF dilute solution. Moreover, the presence of two distinct regimes at ~3 and 10 equiv of D_2O/57ECA might suggest the formation of defined structures with preferred association patterns between water and surfactant amines.

To better elucidate the effect of water and SWNTs on the ^{1}H spin−lattice relaxation dynamics of 57ECA, we performed T_1 measurements as a function of proton number (H_n) and sample temperature (0, 27, and 57 °C). With an exception of H_{10}, Figure 6 plots the average T_1 values in a sequential manner, with the H_1 proton (adjacent to the amine) left and the H_{20} to the right. For neat 57ECA, and in the absence of water (Figure 6A), the central protons exhibit lower T_1 values as opposed to both termini. This is typical for long alkyl chains.[38,39] These values steadily increase with increasing temperature.[40] The addition of 200 μL of water (Figure 6B), which is in the plateau regime of H_1 chemical shift (Figure 5), have caused the following effects to the T_1 values of 57ECA: (i) In the case of 0 and 27 °C experiments, all values are nearly half of that of neat 57ECA; (ii) The T_1 value of H_1 is more significantly depressed than that of H_{20}, and closer to the values of the central surfactant portion; (iii) A large increase in T_1 values is observed for the 57 °C experiment. Here, the T_1 value of terminal H_{20} raises to match or slightly exceed that of the neat 57ECA, while the H_1 value increases from 0.5 to 0.67 of the neat 57ECA. These trends indicate H_2O assists the self-organization of 57ECA and preferentially interacts with the amine group, thereby restricting H_1 mobility. Moreover, a phase-transition appears to take place between 27 and 57 °C, which is beyond the scope of this investigation.

In the presence of SWNTs (Figure 6C) an additional reduction in T_1 values is witnessed, particularly with the 27 and 57 °C curves. Here, due to nanotube immobilization, the H_1 proton is absent (*vide supra*) and it is important to recognize that the T_1 value from the $H_2/H_3/H_{10}$ composite peak might be dominated

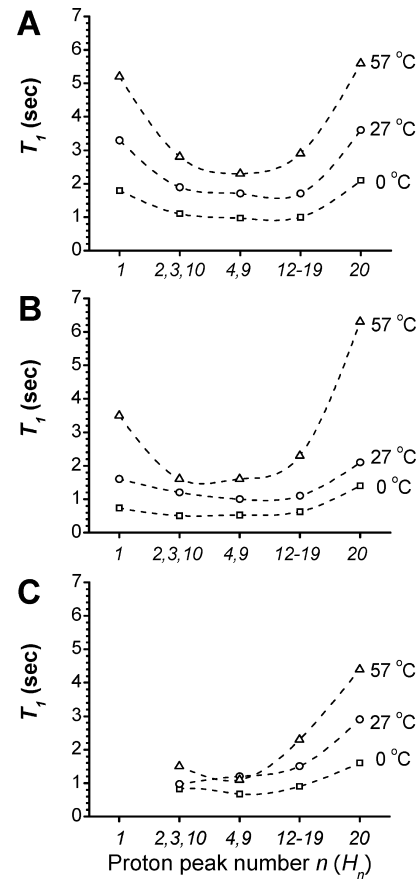

Figure 6. 57ECA ^{1}H NMR T_1 as a function of proton number (H_n) and sample temperature in the absence (A) and presence (B) of water, as well as in the presence of SWNTs (C). Dashed curves were drawn to guide the eye.

by the H_{10} proton, which is the farthest away from the nanotube. Nevertheless, the remaining proton T_1 values paint a consistent picture with increase mobility as we move away from the nanotube. Unlike the 57ECA−H_2O case, the tail mobility increases gradually with temperature while retaining their strong nanotube association (*vide supra*).

To further elucidate the gradual increase in surfactant chain mobility from C_1 to C_{20} we investigated the ^{13}C NMR spectra in the presence and absence of SWNTs. Figure 7A illustrates the ^{13}C NMR spectrum of neat 57ECA in THF-d_8 (in the absence of H_2O). With the help of ^{1}H−^{13}C HMBC, the chemical shifts of all carbon atoms have been deciphered as labeled in Scheme 2 and Figure 7A. Figure 7C zooms in two sections of Figure 7A and exposes the chemical shifts of C_{10} to C_{17}, as well as C_9 and C_4, which are otherwise too close to be visualized. In a similar fashion, B and D of Figure 7 show the ^{13}C NMR spectrum of 57ECA−SWNTs. In the presence of SWNTs, the chemical shifts of C_1 through C_8 are completely lost within the noise, as indicated by the red arrows in Figures 7B and 7D. Moreover, the amplitudes (line-widths) of C_9 to C_{17} atoms exhibit a progressive increase (decrease) as we move from the ninth to the 17th position (Figure 7D). For amplitude comparison, the two ^{13}C spectra were normalized against the C_{20} peak. When, however, the C_{20} line width are compared, a near 2-fold increase is registered in the presence of SWNTs. These findings provide a comprehensive picture of amine anchoring onto the nanotube sidewalls. The gradual line width decrease as the carbon atom moves further from the nanotube depends on the surfactant stiffness and the progressively larger free volume that

(38) Oku, K.; Watanabe, H.; Kubota, M.; Fukuda, S.; Kurimoto, M.; Tsujisaka, Y.; Komori, M.; Inoue, Y.; Sakurai, M. *J. Am. Chem. Soc.* **2003**, *125*, 12739–12748.
(39) Kobayashi, H.; Yoshida, M.; Maeda, I.; Miyashita, K. *J. Oleo Sci.* **2004**, *53*, 105–108.
(40) Sanders, J. K. M.; Hunter, B. K. *Modern NMR Spectroscopy: A Guide for Chemists*; Oxford University Press: New York, 1987.

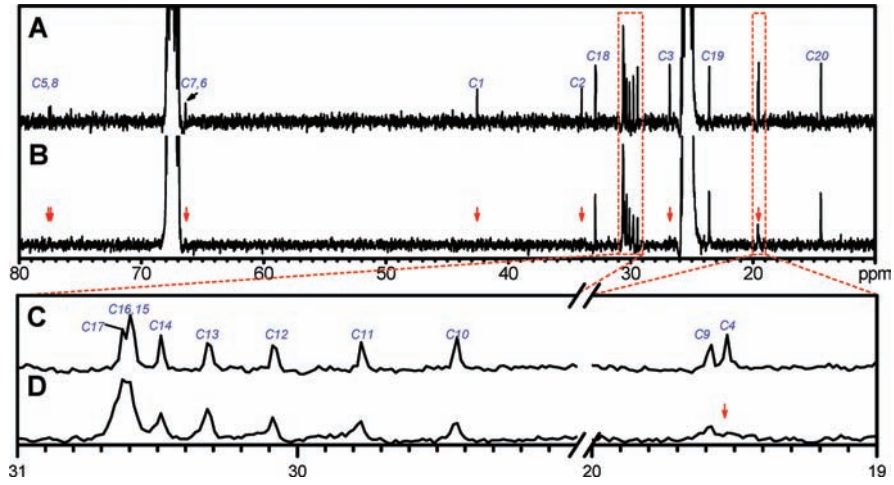

Figure 7. ^{13}C NMR spectra of 57ECA in the absence (A and C) and presence (B and D) of SWNTs. (C) and (D) are close-ups of the respective spectral regions enclosed in dotted boxes in (A) and (B).

the surfactant experiences at greater distance from the graphene sidewalls. In terms of the C_1 to C_8 carbons, the slow tumbling rate of nanotubes in conjunction with the stiff diacetylenic group is believed to account for the loss of their signatures due to broadening.[21] Starting from C_9, the spectral lines are visible, but noticeably broadened compared to the free surfactant. This effect is more pronounced for carbons closer to the headgroup.

Discussion

The NMR results are indicative of strong affinity of the amine head for the sidewalls of SWNTs, with the surfactant tail gaining progressive mobility as it gets further from the nanotube surface. Based on ^{1}H NMR T_1 results, it appears that the interaction with water also diminishes the mobility of the amine head, in a similar fashion with SWNTs, albeit to a lesser degree. Yet the question remains on how a hydrophobic entity like a nanotube is capable to bind to terminal amines in a way similar to water? A crucial piece of information to help us address this question is believed to originate from the acidity of water in the vicinity of SWNTs. It has been shown before by our group[14] as well as others,[41,42] that H_2O actively participates in the electrochemistry of SWNTs. In the presence of acid and O_2, carbon nanotubes loose electrons to produce oxidized, *p*-doped SWNTs ($SWNT^{n+}$), according to reaction 1.[14,41]

$$\mathrm{SWNT} + n\mathrm{H}^+ + \frac{1}{4}n\mathrm{O}_2 \rightleftharpoons \mathrm{SWNT}^{n+} + \frac{1}{2}n\mathrm{H}_2\mathrm{O} \qquad (1)$$

In the presence of water and proton-withdrawing species (like amines), reaction (1) was shown to reverse its course and produce undoped or less *p*-doped SWNTs.[14] For SWNTs with diameter ($d_t = 1.0$ nm), where *sem*- from *met*-SWNT separation was shown experimentally[2,13] and by modeling[14] to reach maximum, exposure to a mixture of HNO_3/H_2SO_4 provides a depth of doping at *ca.* 0.04 and 0.01 electrons/carbon atom per *sem*- and *met*-SWNTs, respectively (Figure S7 in SI). This implies that a counterion (i.e., NO_3^-) and its hydration sphere (*ca.* 5 H_2O molecules[29]) needs to come in close proximity with either 25 carbon atoms of *sem*-SWNTs or with 100 carbon atoms of *met*-SWNTs. In accordance with reference,[29] a two-dimensional (2D) close-packed arrangement of hydrated NO_3^- ions produces an intermolecular nitrate spacing of *ca.* 5.2 Å, shown in the left part of Figure 8A. Such 2D-arrangement of NO_3^- ions covers *ca.* 8 graphene carbons per hydrated nitrate, which is much less from the aforementioned 25 carbons per one electron doping of *sem*-SWNTs. This 2D arrangement creates a strong driving force for small bundling (i.e., three *sem*-nanotubes in a bundle), which is capable of accommodating both continuous counterions/hydrate and the hydrophobic sidewall remainders of SWNTs (shown in the right part of Figure 8A). Assuming that nanotube bundling allows for charge distribution through all participating nanotubes,[43] a small bundle of three *sem*-SWNTs with $d_t = 1.0$ nm exposes ~8 to 9 carbon atoms per counterion. This is in agreement with both simulation and experimental results, provided by XRD and HRTEM (Figures 3B and S1), respectively.

When the hydrated, close-packed $NO_3^-/(H_2O)_5$ 2D arrangement is presented to surfactant amines, the inverse of reaction (1) takes place as a result of acid neutralization. Since the molar volume of NH_4^+ ions is shown to be comparable to that of H_2O (in terms of bond angles, interatomic distances, and hydrogen bonding)[44] the replacement of surfactant amine with water is expected to occur with minimum change in the average molecular arrangement.[45] If such neutralization is driven to completion, reaction (2) is expected for 25 carbon atoms equivalence of a nanotube (or 8.33 surface carbons per small bundle of three nanotubes) (Figure 8B).

$$\mathrm{SWNT} + /(\mathrm{NO_3^-}) + 5\mathrm{H_2O} + \mathrm{RNH_2} \rightleftharpoons \mathrm{SWNT^+RNH_3^+}/(\mathrm{NO_3^-}) + 4.5\mathrm{H_2O} + 0.25\mathrm{O_2}\uparrow \qquad (2)$$

The well-known affinity of O_2 for hydrophobic entities is expected to remove the generated oxygen away from the nanotube surface, leaving behind a 2D hydrophilic layer that has been augmented by an amine and depleted by a half-water molecule. Molecular simulations indicate that this corresponds to an approximate 10 to 11% volume increase in the hydrophilic 2D-layer that surrounds the small *sem*-SWNT bundles, since

(41) Zheng, M.; Diner, B. A. *J. Am. Chem. Soc.* **2004**, *126*, 15490–15494.
(42) O'Connell, M. J.; Eibergen, E. E.; Doorn, S. K. *Nat. Mater.* **2005**, *4*, 412–418.
(43) Baughman, R. H.; Cui, C.; Zakhidov, A. A.; Iqbal, Z.; Barisci, J. N.; Spinks, G. M.; Wallace, G. G.; Mazzoldi, A.; De Rossi, D.; Rinzler, A. G.; Jaschinski, O.; Roth, S.; Kertesz, M. *Science* **1999**, *284*, 1340–1344.
(44) Vollmar, P. M. *J. Chem. Phys.* **1963**, *39*, 2236–2248.
(45) Narten, A. H. *J. Phys. Chem.* **1970**, *74*, 765–768.

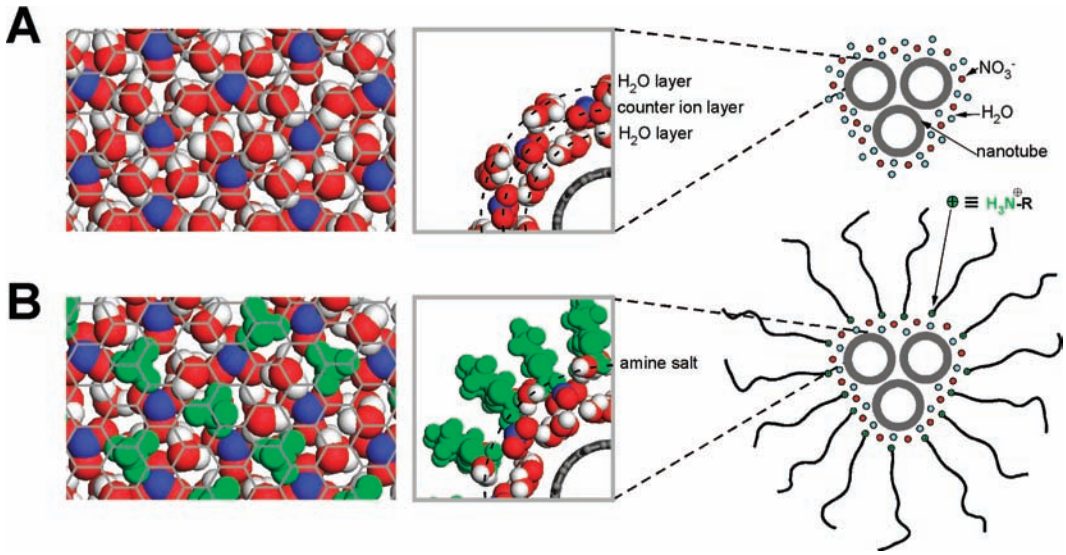

Figure 8. Molecular simulation arrangement of hydrated nitrate counterions, in the absence (A) and presence (B) of the surfactant amine. N, O and H are shown in blue, red and white, respectively, while the surfactant amine is shown in green. (Left) 2D arrangements of NO_3^- ions on top of a graphene lattice. For clarity purposes, only the H_2O molecules adjacent to the graphene lattice are shown. (Center) Edge views of hydrated NO_3^- ions (A) and surfactant amine salts (B). (Right) Schematic representation of 2D organization around small nanotube bundles containing three SWNTs.

one molecule of H_2O is replaced with two -NH_3^+ moieties. Moreover, the need for the surfactant amine head to get in close proximity of the NO_3^- ions exerts a substantial compression of the hydrophilic 2D-layer by its hydrophobic tail. Such compression is currently believed to lead in less than complete neutralization. For example, a 95% neutralization will leave 0.025 H_3O^+ per 462.5 H_2O, assuming that the equilibrium constant of reaction (1) is unity. This corresponds to a 2.26 localized pH of the water in the vicinity of SWNTs, which is in good agreement with the NMR results of Figures 4 and S5 in SI. Such low pH is expected to retain significant part of the *p*-doped nature of SWNTs,[46] and account for strong interactions of the graphene sheet with the adjacent charge-balancing NO_3^- counterions. In addition, the surfactant-driven compressive force around the hydrophilic 2D-layer is expected to shield it from the surrounding amine-driven basic environment and retain its acidic nature.

The partial neutralization of surface acidity of *p*-doped SWNTs provides a more comprehensive picture of the surfactant amine-assisted enrichment of *sem*-SWNTs. First and foremost it indicates that the extraordinary stability of the (*sem*-SWNT)$_3$/surfactant amine complex might originate from the regular 2D pattern of alternating NO_3^- and RNH_3^+ groups that are interspaced with acidic water (Figure 8B left). Moreover, the enrichment of *sem*- against *met*-SWNTs appears to originate not from the action of amines but rather the inherent redox differences between the *sem*- and *met*-SWNT species. Unlike the well-distributed 2D arrangements of $NO_3^-/(H_2O)_5$ and $NO_3^-/RNH_3^+(H_2O)_{4.5}$ around a small bundle of three *sem*-SWNTs, similar bundling arrangements between various mixtures of *met*- and *sem*-SWNTs can never be established due to: (i) inability of *met*-SWNTs to attain as large charge/carbon ratio, and (ii) progressively higher resistance for outer surface charge redistribution as the bundle size increase.[43] For bundle mixtures of *met*- and *sem*-SWNTs, this ideal 2D arrangement of NO_3^-, RNH_3^+ and H_2O is disturbed. This is expected to cause a discontinued, patch-like surfactant decoration on the surface of the nanotube bundles containing *met*- and *sem*-SWNTs mixtures. Such action depresses the ability to *met*-containing SWNT bundles to disperse in THF that ultimately leads to *sem* enrichment. Having said this, it is important to stress that the kinetics of the formation of these small, *sem*-enriched, SWNT bundles in the present of surfactant amines are currently unknown, which warrants the topic of a separate study.

Conclusion

Both static and dynamic characteristics of surfactant amine organization on the surface of SWNTs were investigated using an asymmetrical diacetylene-based surfactant amine (57ECA), presenting a similar *sem* enrichment to that of octadecylamine (ODA). Despite the nonbonding arrangement of the surfactant with SWNTs, ^1H and ^{13}C NMR investigations indicate that the amine headgroup is firmly immobilized onto the nanotube surface together with acidic water, while the tail attains progressively larger mobility as it gets farther from the SWNT. High resolution transmission electron microscopy in conjunction with X-ray diffraction results point toward the fact that the *sem*-enriched fraction is populated by small nanotube bundles containing approximately three SWNTs. With the help of molecular modeling and previously published differential oxidation depths for *sem*- and *met*-SWNT species, the formation of these small, *sem*-enriched bundles were explained on charge redistribution on the surface of these bundles together with the formation of a stable 2D arrangement of NO_3^-/surfactant amine/water layer. The significantly less oxidation depth of *met*-SWNTs renders the aforementioned arrangement discontinuous around the nanotube bundles, thereby explaining their inability for THF dispersion. This study provides a comprehensive picture of the surfactant amine-assisted *met*- from *sem*-enrichment methodology, explains its profound differences from other separation techniques, and further enhances our understanding of the complex molecular interaction at the surface of redox-prone nanomaterials.

(46) Strano, M. S.; Huffman, C. B.; Moore, V. C.; O'Connell, M. J.; Haroz, E. H.; Hubbard, J.; Miller, M.; Rialon, K.; Kittrell, C.; Ramesh, S.; Hauge, R. H.; Smalley, R. E. *J. Phys. Chem. B* **2003**, *107*, 6979–6985.

Acknowledgment. We thank Dr. Martha Morton and Dr. Rongfu Li for helpful discussions and setup on NMR experiment and TEM measurement, respectively. Financial support, mainly from AFOSR FA9550-06-1-0030NSF, and in part by NSF-NIRT DMI-0422724, and NSF-CBET-0828771/0828824, NIH ES013557 is greatly appreciated.

Supporting Information Available: High-resolution transmission electron microscopy (HRTEM) images of 57ECA−SWNTs (Figure S1), 2D $^{1}H-^{1}H$ COSY (Figure S2), 2D $^{1}H-^{13}C$ HMBC (Figure S3), and close-up of $^{1}H-^{13}C$ HMBC (Figure S4) of neat-57ECA along with assignments of peaks, acidity effects on the ^{1}H NMR position of water peak of 57ECA (Figure S5), confirming the absence of buried peak under water using temperature-controlled ^{1}H NMR (Figure S6), and valence density of states (DOS) with respect to vacuum for a (7,7)-*met*- and (11,3)-*sem*-SWNTs (Figure S7). This material is available free of charge via the Internet at http://pubs.acs.org.

JA809054C